Int J Adv Manuf Technol (2016) 87:1967–1975
DOI 10.1007/s00170-016-8594-4

ORIGINAL ARTICLE

Prediction of grinding force for brittle materials considering co-existing of ductility and brittleness

Chongjun Wu[1,2] · **Beizhi Li**[1] · **Jianguo Yang**[1] · **Steven Y. Liang**[2]

Received: 20 October 2015 / Accepted: 2 March 2016 / Published online: 14 March 2016

Abstract Grinding of brittle materials is characterized by a complex removal mechanism of both ductile and brittle removal. Therefore, the traditional force models, which are mainly targeted to metallic materials, cannot be fully applied to the force prediction of brittle materials. This paper will propose a new grinding force model for brittle materials considering co-existing of ductile removal force and brittle removal force. The ductile removal force is mainly composed of rubbing force, ploughing force, and chipping force. However, the brittle removal force is more related to rubbing force and fracture chipping force. The proportional coefficient of ductile removal and crack size will be modeled through a series of experiments under different wheel speed and undeformed chip thickness. The working status for a single grit was separated based on the Hertz Theory and chip thickness modeling of Rayleigh probability density function. Grinding experiments have been undertaken by using a high speed diamond grinder on Silicon Carbide, and the results was compared to the force model predictions for validation. The predictive force model shows a reasonable agreement quantitatively with the experimental force data.

✉ Chongjun Wu
wcjunm@126.com

Beizhi Li
lbzhi@dhu.edu.cn

Jianguo Yang
jgyangm@dhu.edu.cn

Steven Y. Liang
steven.liang@me.gatech.edu

[1] Donghua University, Shanghai, China

[2] Georgia Institute of Technology, Atlanta, GA, USA

Keywords Grinding force · Brittle materials · Ductile grinding · High speed grinding

1 Introduction

During the last decades, the demand for high-precision ceramic parts has been increasing continuously for their high strength, wear resistance, and good chemical stability [1]. Such ceramic parts have been used into a wide range of applications in the high-end optical components, micro mechanical parts, and communication industry as well as in medical and life sciences [2, 3]. In recent research publications, grinding has become one of the most productive methods for precision machining of brittle materials, such as Al_2O_3 [4], SiC [2, 4], glasses [3], etc. However, it still shows great difficulty to machine them because of their great hardness and brittleness. Grinding with diamond wheels [5, 6] has become the main processing method that can be expected to achieve the desired dimensional tolerance and surface integrity. Moreover, the machine tools being used to machine brittle materials are characterized by closed loop structure, high accuracy, and excellent rigidity [7, 8].

The grinding forces are very important quantitative parameters to characterize the material removal mode and determine the grinding energy in grinding of brittle materials. The ability to predict grinding force and power is important to many aspects of grinding process optimization, monitoring, and control [9]. Malkin et al. [10] have proposed that grinding forces were composed of cutting deformation force and sliding force based on experimental results about the relationship between grinding force and grinding wheel abrasion plane area, but no formula on tangential grinding force was put forward. Badger et al. [11] proposed two kinds of grinding force model, the first model based on Challen and Oxley's

two-dimensional (2-D) plane-strain slip-line field theory, the second model based on Williams and Xie's three-dimensional (3-D) pyramid-shaped asperity model. These two models simulated the grit–workpiece interface to a rigid plastic contact, and mechanical behavior of this kind of contact was influenced by the grit slope and interfacial coefficient of friction between the asperity and the worn material. Another different grinding force model was proposed by Hecker et al. [9]. In his model, the chip thickness was assumed as a Rayleigh probability density distribution. Afterwards, Patnaik et al. [12] proposed a grinding force model which is based on the fact that chip formation during grinding consists of three stages: rubbing, ploughing, and cutting. While rubbing is associated with elastic deformation, ploughing is plastic deformation or where majority of the material is displaced without being removed and cutting where removal of material takes in the form of miniature chips. However, because of different material removal mechanism between metallic and brittle materials, the above models cannot be fully applied to grinding of brittle materials.

Usually, grinding of hard and brittle materials causes a great deal of microcracks which deteriorate surface quality [7]. Moreover, the material removal for grinding of brittle materials is mainly associated with rubbing and fracture cracking. While for the metallic materials, rubbing, ploughing, and chipping are the main processes for material removal. Thus, the transition from brittle to ductile material removal is considered to be of great importance for precision grinding of brittle materials. Much research effort has been spent to identify this transition and to understand the removal mechanism based on the critical chip thickness model proposed by Bifano [13]. Bifano has indicated that in the machining of brittle materials ductile grinding could be achieved when the maximum undeformed chip thickness is less than a critical chip thickness. However, this model was established under conventional wheel speed (26.2 m/s) and does not apply for high speed grinding, there still lack of a quantitative description of ductile grinding of brittle materials considering strain rate which is caused by wheel speed.

From the above literature review and analysis, it indicates that grinding of brittle materials will experience both ductile and brittle grinding. Therefore, the predictive grinding force models for brittle materials should fully consider both of the two material removal mechanisms. This paper will propose a novel force model for grinding of brittle materials, incorporating both ductile removal force and brittle removal force. A series of experiments will be conducted to model the proportional coefficient of ductile removal under different wheel speed and undeformed chip thickness. Moreover, the ductile removal force will be predicted based on the generation of rubbing force, ploughing force, and chipping force, while the brittle removal force will be more related to rubbing force and fracture chipping force. The working status for abrasive grit will be separated based on the Hertz Theory and chip thickness modeling of Rayleigh probability density function. Finally, grinding experiments will be undertaken to calibrate and validate the predictive model. The model helps in predicting grinding forces for brittle materials without having to resort to experimental techniques.

2 Grinding force modeling

In grinding processes, brittle materials will be removed by both ductile and brittle mode. Therefore, the grinding forces will be divided into two categories. When the grit interacts with the workpiece, if the ground workpiece surface is mainly conducted by ductile flow the ductile grinding is the main removal mode, the corresponding grinding force is composed by rubbing force, ploughing force, and chipping force. While when the ground workpiece surface is mainly conducted by fracture cracks, the brittle fracture grinding is the main removal mode, the grinding force is mainly comprised of rubbing force and fracture chipping force.

$$F = \delta F_{ductile} + (1-\delta) F_{brittle} \tag{1}$$

$$F_{\text{ductile}} = F_{\text{drubbing}} + F_{\text{dploughing}} + F_{\text{dchip}} \tag{2}$$

$$F_{\text{brittle}} = F_{\text{brubbing}} + F_{\text{bchip}} \tag{3}$$

where δ is a percentage proportional constant, which is determined by the removal mode of ground surface.

2.1 Chip thickness model

The chip thickness is a very important quantitative indicator in process planning and model construction. In this paper, considering the stochastic distribution of grits, the chip thickness was assumed to conform to the Rayleigh distribution [9, 14]. The grinding chips can be formed only when the undeformed chip thickness h is between the minimum chip thickness h_{cr} and maximum chip thickness $h_{\max}$.

$$f(h) = \begin{cases} \left(h \Big/ \sigma^2\right) e^{-h^2/2\sigma^2} & h_{\text{cr}} \le h \le h_{\max} \\ 0 & h \le h_{\text{cr}}, h \ge h_{\max} \end{cases} \tag{4}$$

where σ is a parameter that fully defines the Rayleigh probability function. h_{cr} is the minimum chip thickness, when a single grit has a theoretical chip thickness smaller than h_{cr} the grinding chips will not be formed and h_{cr} varies under different operation parameters. While $h_{\max}$ is the maximum chip thickness, only when a single grit has a theoretical chip thickness smaller than the $h_{\max}$, the grinding chips may be

produced. The maximum chip thickness [6] can be defined in the following formula.

$$h_{\max} = \left(\frac{3}{C_d.\tan(\theta)}.\frac{V_w}{V_s}.\sqrt{\frac{a_e}{d_e}}\right)^{\frac{1}{2}} \quad (5)$$

where C_d represents the active abrasive grits number in unit area, which reflects the grit density. a_e the depth of cut. V_s and V_w, respectively, represents the wheel speed and workpiece peripheral speed. Different shapes for abrasive grit have been approximated to simplify the analysis of individual interaction with the workpiece material. In this part, a conical shape [9, 12] will be chosen for mathematical simplification. The semi-included angle of the active grit θ is 60°. The value of C_d, in Eq. (5), can be obtained by a simple geometric relationship derived by Xu et al. [15], can be given as follows [14, 15].

$$C_d = 4\chi/\left\{d_g^2(4\pi/3\omega)^{2/3}\right\} \quad (6)$$

where d_g is the equivalent spherical diameter of diamond grit, ω is the volume fraction of diamond in the grinding wheel, and χ is the fraction of diamond particles that actively cut in grinding. The grinding wheel used in this paper has a density of 150, or in other words, volume fraction ω is 0.375 [16]. To obtain the value of C_d, it is assumed that only one-third of the diamond particles on the wheel surface are actively engaged in cutting, or the value of χ is equal to 1/3 [4]. Considering the grit size of 91 μm, C_d is 32/mm^2, which is close to the SEM observations results [17] of 30/mm^2 with the same grinding wheel. The actual grits number when the grinding wheel interacts with the workpiece materials can be calculated through the product of grits density C_d and contact area square [9, 14].

$$N_d = C_d.l_g.b \quad (7)$$

where N_d represents the overall grit number under different operation parameters, l_g the contact arc length and can be calculated through $l_g = \sqrt{d_s \cdot a_e}$ [18]. b is the minor value between the width of the wheel and workpiece.

The chip thickness model will be valid only when the integration is equal to 1.

$$\int_{h_{\mathrm{cr}}}^{h_{\max}} f(h)dh = 1 \quad (8)$$

Hecker et al. [9] have put forward the following equations through the total material removal volume. The removed material volume by grinding wheel is equal to the lost material volume of the workpiece.

$$E(A_{\mathrm{total}})V_S = V_w a_e b \quad (9)$$

In grinding processes, the workpiece will undergo rubbing, ploughing, and chipping process [12]. During the ploughing action, the material was pushed moving aside leading the cross section larger than the undeformed cross section area. Subhash et al. [19] proposed an expression for the critical strain at which the strength becomes significantly strain-rate dependent. It can be expressed as $\sigma_c = E \cdot \varepsilon$ [20]. For SiC in their work [20], the critical strain ε was 1.1 % (compression strength $\sigma_c = 5.0$GPa and elastic modulus $E = 440$GPa). Therefore, because of the high elastic modulus for ceramic workpiece, a very small deformation will be produced during grinding. Thus the ploughing effect will not be considered in the calculation of the cross section area. The total material removal volume can be calculated through the product of theoretical undeformed triangle cross section and the active grits number. It can be given as follows.

$$A_{\mathrm{total}} = A_{\mathrm{chip}}.N_d \quad (10)$$

$$A_{\mathrm{chip}} = h^2.\tan\theta \quad (11)$$

where A_{total} represents the total chip triangle cross section when the whole grinding wheel interacts with the workpiece. A_{chip} is the chip triangular cross section for a single grit. Therefore, the expected value of the total cross section E (A_{total}) can be expressed in the following equation.

$$E(A_{\mathrm{total}}) = N_d E\left(A_{\mathrm{chip}}\right) = N_d E\left(h^2\right).\tan\theta \quad (12)$$

Through substituting and elimination of $E(A_{\mathrm{total}})$ in Eqs. (9) and (12),

$$E\left(h^2\right) = \frac{V_w a_e b}{V_s N_d \tan\theta} \quad (13)$$

And $E(h^2)$ can be obtained through integral calculation.

$$E\left(h^2\right) = \int_{h_{cr}}^{h_{\max}} h^3/\sigma^2 e^{-\frac{h_{cr}^2}{2\sigma^2}} dh = 2\sigma^2 + h_{cr}^2 e^{-\frac{h_{cr}^2}{2\sigma^2}} - h_{\max}^2 e^{-\frac{h_{\max}^2}{2\sigma^2}} \quad (14)$$

Therefore, h_{cr} and σ can be obtained through the solution of Eqs. (8) and (13).

2.2 Force components for ductile grinding

2.2.1 Determination of grit working status

In order to simplify the analysis of the single grit interaction with the workpiece material, the cutting edge shape will be approximated, to be assumed, to a spherical shape [11, 16] in the determination of grit working status. Earlier researchers [21] have applied Hertz theory to grinding process to estimate the depth of indentation when the abrasive grit is pressed against the flat workpiece. According to Hertz theory, the maximum stress on the contact area ($\sigma_{\max}$) for elastic contact between a sphere of radius (R_g) and a flat surface can be evaluated from the following Eq. (15). In this paper, the diameter of the workpiece is 60 mm, compared with a diameter

of 91 μm for abrasive grit. Therefore the equivalent radius R_e can be calculated through $1/R_e = 1/R_g + 1/R_w$ [22], which is very close to the abrasive grit radius. Here R_g represents the radius of the abrasive grit, R_w the workpiece radius.

$$\sigma_{\max} = 0.5784^3 \sqrt{\frac{F_{\mathrm{gr}}}{{R_g}^2 \left(\frac{1-{\mu_{\mathrm{SiC}}}^2}{E_{\mathrm{SiC}}} + \frac{1-{\mu_{\mathrm{diamond}}}^2}{E_{\mathrm{diamond}}}\right)^2}} \tag{15}$$

where F_{gr} is the load on the grain, μ_{SiC} and μ_{diamond} are the Poisson rate of SiC and diamond, and E_{SiC} and E_{diamond} are the elastic modulus of SiC and diamond, respectively.

While the depth of indentation for elastic loading is given by:

$$\zeta = 0.8255^3 \sqrt{\left(\frac{1-{\mu_{\mathrm{SiC}}}^2}{E_{\mathrm{SiC}}} + \frac{1-{\mu_{\mathrm{diamond}}}^2}{E_{\mathrm{diamond}}}\right) \frac{{F_{\mathrm{gr}}}^2}{R_g}} \tag{16}$$

The grinding process is a complex process between the abrasive grit and the material, and different abrasive grits have a different working rake angle. Therefore, the material will experience a continuous changing force when interaction with the grit. The maximum stress $\sigma_{\max}$ will be at the onset of plastic deformation and is equal to bending strength of the workpiece material. Substituting this value for $\sigma_{\max}$ and eliminating F_{gr} in Eqs. (14) and (15), the depth of indentation will be achieved when elastic loading is applied. Thus, different working status of the interaction between the grit and workpiece can be acquired by introducing the minimum chip thickness h_{cr} and maximum chip thickness $h_{\max}$. When the chip thickness is between these two chip thicknesses, the grinding chips can be formed. While when the depth of interaction is lower than the critical chip thickness h_{cr} and higher than the depth under elastic loading the ploughing stage is dominated. And the pure elastic stage in hertz contact is the rubbing process.

$$\begin{aligned} &0 < h < \zeta, && \text{rubbing} \\ &\zeta < h < h_{\mathrm{cr}}, && \text{ploughing} \\ &h_{\mathrm{cr}} < h < h_{\max}, && \text{chipping} \end{aligned}$$

2.2.2 Force components for ductile grinding

The rubbing stage is mainly associated with elastic deformation. When the single grit interacts with the material, the elastic loading will be the most dominant force source. According to the Hertz theory and formula (15), the rubbing force under elastic loading can be given as below. In this formula, the rubbing force is half of the maximum rubbing force.

$$F_{\mathrm{drubbing}} = \frac{\zeta}{2}.k_1.N_d.F_{\mathrm{gr}} = \zeta.k_1.N_d.{\sigma_{\max}}^3 {R_g}^2 \left(\frac{1-{\mu_{\mathrm{SiC}}}^2}{E_{\mathrm{SiC}}} + \frac{1-{\mu_{\mathrm{diamond}}}^2}{E_{\mathrm{diamond}}}\right)^2 \tag{17}$$

where k_1 is a constant which is determined through experiments.

While when the chip thickness is higher than the depth of indentation for elastic loading and lower than the critical chip thickness, the plastic deformation will be the main interaction mode. During this phase, the grinding chips will not be formed and the scratching striation will be the main interaction result. De Vathaire et al. [23] proposed an upper bound model of ploughing by a pyramidal indenter and the experiments were conducted on a low carbon steel workpiece. In the ploughing phase, the workpiece material will bear the maximum resistance of the workpiece hardness. And the action area is the chip cross section A_{chip}. The ploughing force can be given as:

$$F_{d\mathrm{ploughing}} = k_2.N_d.Hv.A_{\mathrm{chip}} = k_2.N_d.Hv.\left(\frac{h_{cr}-\zeta}{2}\right)^2.\tan\theta \tag{18}$$

where k_2 is a material constant which is determined by experiments, Hv the Vikers hardness.

When the depth of interaction is between the two critical indicators h_{cr} and $h_{\max}$, the grinding chips can be formed and ductile removal and brittle removal are both acting in the grinding process. If the depth of indentation keeps increasing to a higher value above the maximum chip thickness, the grinding chips will be mainly characterized by fracture cracks and brittle removal will be the only mode. According to Vickers indention experiments, the minimum threshold load is what makes the brittle and hard material to just fracture. Therefore, the chipping force under ductile removal can be approximated to this threshold load. It can be given as below.

$$F_{d\mathrm{chip}} = k_3.N_d.\left({K_{1C}}^4/Hv^3\right) \tag{19}$$

where k_3 is a constant which is dependent on the wheel topology and material, it is determined through experiments.

2.3 Force components for brittle grinding

Because of the hard and brittle nature of brittle materials, the removal of the materials is more tended to be irregular fracture cracks at a high material removal volume. In the brittle removal of the brittle materials, the workpiece material will first experience elastic loading as in ductile grinding. Then the plastic deformation will be the main interaction stage. During this stage, the grinding chips will be formed in the means of fracture cracks. Therefore, the grinding force will be mainly comprised of rubbing force and fracture chipping force in ductile grinding. The rubbing force in brittle grinding will be equal to the force in ductile grinding.

$$F_{b\mathrm{rubbing}} = \frac{\zeta}{2}.k_4.N_d.F_{\mathrm{gr}} = \zeta.k_4.N_d.{\sigma_{\max}}^3 {R_g}^2 \left(\frac{1-{\mu_{\mathrm{SiC}}}^2}{E_{\mathrm{SiC}}} + \frac{1-{\mu_{\mathrm{diamond}}}^2}{E_{\mathrm{diamond}}}\right)^2 \tag{20}$$

where k_4 is a material constant which is determined through experiments. In indentation experiments, Lawn

[24] gave the connection between crack size C and load P through modeling the area under the indentor as a plastic expansion area.

$$P/C^{3/2} = K_{1C}/\left\{\xi(\cot\theta)^{2/3}(E/Hv)^{1/2}\right\} \tag{21}$$

where ξ is a constant, E is the elastic modulus of material. Therefore, the chipping force model should be the following formula.

$$F_{b\text{chip}} = k_5.N_d.C^{3/2}.K_{1C}/\left\{(\cot\theta)^{2/3}(E_{\text{SiC}}/Hv)^{1/2}\right\} \tag{22}$$

where k_5 is a constant which is determined through experiments. It can be found from the above model that the brittle chipping force is not only concerned with the material properties, also highly related to the fracture crack size.

2.3.1 Force orientation

Hecker at al. [25] proposed the tangential and normal force calculation formula based on the Brinell hardness. The calculation method was given as below.

$$\begin{aligned} F_t &= F(\sin\phi + f\cos\phi) \\ F_n &= F(\cos\phi - f\sin\phi) \end{aligned} \tag{23}$$

where f is the friction coefficient between the grain and the workpiece and Φ is the effective angle [9], which is related to the undeformed chip thickness h and grain affective grit radius R_g. When the grit is in different grinding stage, a different depth h will lead to a different effective angle.

$$\phi = \arccos\left(1 - \frac{h}{R_g}\right) \tag{24}$$

Combining the formula (1), (2), (3), and (23), (24), the final normal force and tangential force can be obtained in the following Eq. (25).

$$\begin{aligned} F_n &= \left\{\delta.\left(\overrightarrow{F_{d\text{rubbing}}} + \overrightarrow{F_{d\text{ploughing}}} + \overrightarrow{F_{d\text{chip}}}\right) + (1-\delta).\left(\overrightarrow{F_{b\text{rubbing}}} + \overrightarrow{F_{b\text{chip}}}\right)\right\}.(\cos\phi - f\sin\phi) \\ F_t &= \left\{\delta.\left(\overrightarrow{F_{d\text{rubbing}}} + \overrightarrow{F_{d\text{ploughing}}} + \overrightarrow{F_{d\text{chip}}}\right) + (1-\delta).\left(\overrightarrow{F_{b\text{rubbing}}} + \overrightarrow{F_{b\text{chip}}}\right)\right\}.(\sin\phi + f\cos\phi) \end{aligned} \tag{25}$$

3 Experimental set-up

Grinding experiments were carried out on the MGKS1332/H CNC cylindrical grinding machine. The machine spindle is capable of running up to 8000 rpm with a 400-mm wheel. The workpiece material used for this investigation was SiC, whose properties are given in Table 1. The workpiece specimens have the diameter of 60 mm with the length of 20 mm. A vitrified diamond grinding wheel, with an average grit size of 80 μm, diamond concentration of 150 %, diameter 400 mm and width 22 mm, was used. The diamond grit has a density of 3.56 g/cm^3 and Poisson rate 0.16. The wheel was balanced below 0.02 μm at the grinding speed with a dynamic balancing instrument (Model SB-4500). A series of shallow plunge grinding experiments will be developed in this paper. The grinding wheel was trued using a diamond truer and dressed using an alumina stick of 200 mesh size for 30s under coolant before every set of test was undertaken. The truing ratio for the grinding wheel is 0.8 under a wheel speed of 80 m/s, the depth of cut 2 μm, and the transverse feed rate of 400 mm/min. In this paper, a 5 % water-soluble metal cutting fluid was used.

The grinding force detecting device is a 3-direction force transducer (Kistler 9347C) mounted in the tailstock. The transducer is collected to a charge amplifier; then, the collected signal is sent to the data acquisition system LMS. A column workpiece, as shown in the upper right of Fig. 1, is separated into two pieces, a quarter part and the rest.

An environment scanning electron microscope (ESEM) QUANTA 250 from Czech was used to examine the ground surface and subsurface fracture crack size. A bonded interface sectioning technique [26] was used to examine the grinding

Table 1 Mechanical properties for SiC

SiC properties						
SiC	Density	Bending strength	Hardness	Fracture toughness	Elastic modulus	Poisson rate
	ρ_{SiC}	σ_b	Hv	K_{1C}	E_{SiC}	μ_{SiC}
	[g/cm^3]	[MPa]	[GPa]	[MPa.m$^{1/2}$]	[GPa]	[−]
	3.05	430	23	3.0	410	0.16

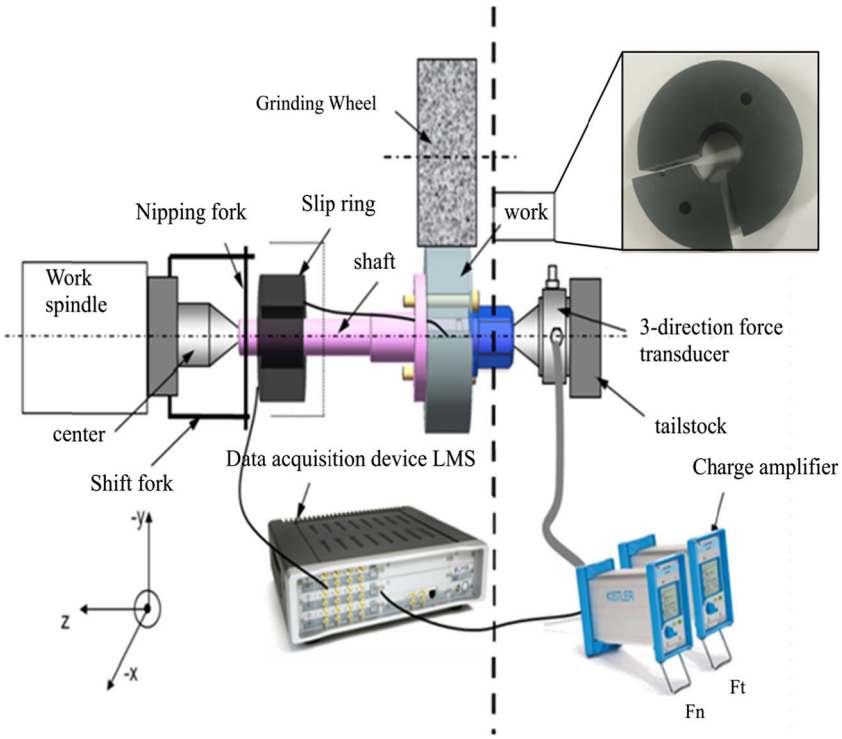

Fig. 1 Grinding force test layout

induced subsurface damage. Two parts of the workpiece were first polished and then bonded together using a cyanoacrylate-based adhesive. Clamping pressure was applied during bonding to ensure that a thin adhesive layer joint was achieved, which would minimize edge chipping during grinding. The grinding direction was perpendicular to the bonded interface. After grinding the bonded specimens were subsequently separated by heating on a hot plate to soften the adhesive. Before the examination, the ground specimens were cleaned with acetone in an ultrasonic bath for at least 20 min, and then gold coated.

4 Model calibration

4.1 Force proportion parameter modeling δ

From the SEM ground surface in Fig. 2, it can be found that the ground surface is characterized by both ductile flow and fracture cracks. This is mainly because of the irregular distribution of abrasive grits and machining process. In ductile grinding, the ground surface is characterized by scratching groove and tiny chips. While in the brittle grinding, the ground surface shows more concave pit generated by fracture cracks. A grid interface sectioning technique [13] was used to quantitatively distinguish brittle area from the whole ground surface. It can be seen from the Fig. 2 that the figure was divided by a 20×20 grid. When the ground surface is dominant by fracture cracks the grid will be marked as red, the percentage of red grids in the Fig. 2 represents the whole proportion of brittle surface in the whole ground surface.

A series of experiments were conducted to establish the proportion parameter model for distinguishing ground surface. The detailed experimental planning is shown in Table 2, No. 1–8 is for the model construction and No. 9–10 is for the validation of this model.

On the basis of the material removal energy [27], Bifano et al. [13] established a critical grinding depth model for ductile grinding of brittle materials. He gave detailed explanation of the grinding depth effect on machining damage. Moreover, Kovach et al. [28] clearly demonstrated that the increase of grinding speed can result in an improved surface finish and lower damage for advanced ceramics. Their results also concluded that a transition from a brittle fracture mode to a low damage ductile grinding mode could be achieved when the wheel speed elevated. Therefore, it is obvious the grinding depth and the wheel speed will have a great effect on the ground quality. Based on the above analysis, the model can be given as below.

$$\delta = \varepsilon (h_{\max})^{\beta} (V_S)^{\kappa} \tag{26}$$

where ε, β and κ are constants which are determined by experiments. Through calculation based on the experimental

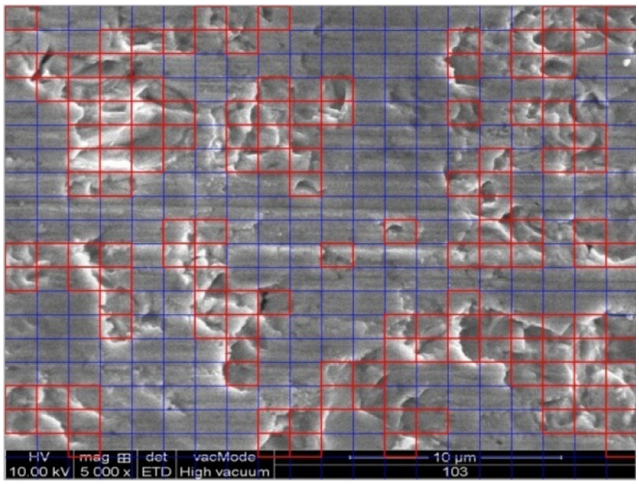

Fig. 2 SEM ground surface characterization using a grid interface sectioning technique

data in Table 1, the real model for the proportion parameter can be written as:

$$\delta = 58.4.(h_{\max})^{-0.357}(V_S)^{-0.024} \tag{27}$$

4.2 Experimental model for crack size C

Similar to the model construction in 5.1, another series of experiments were conducted to establish crack size model for the chipping force modeling of ductile grinding (Fig 3). The detailed experimental planning is shown in Table 3, No. 1–8 is for the model construction and No. 9–10 is for the validation of this model. Based on the speed effect and grinding depth effect on the grinding cracks, the model was given as follows:

$$C = \varepsilon'(h_{\max})^{\beta'}(V_S)^{\kappa'} \tag{28}$$

where ε', β' and κ' are constants which are determined by experiments. Through calculation based on the experimental data

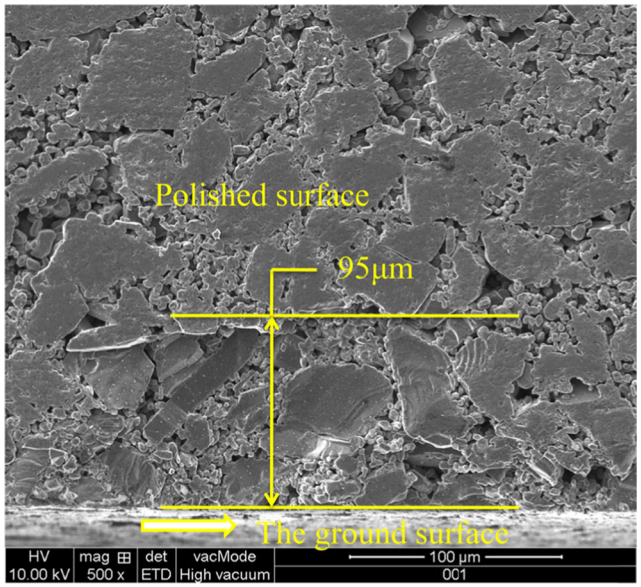

Fig. 3 SEM ground subsurface damage quantitative characterization

in Table 1, the real model for the proportion parameter can be written as:

$$C = 223.(h_{\max})^{0.3}.(V_S)^{-0.275} \tag{29}$$

5 Force model calibration and verification

The final force model was calibrated and validated through a total of 20 different process parameters illustrated in Table 4. The first 12 groups are used for the calibration, the remains are for validation.

After substituting all the parameters into the final force model, the rubbing force in both ductile grinding and brittle grinding is found to be very small comparing to other force components (more than ten orders of magnitude). Therefore, the constants k_1 and k_4 are all given the value 0. While k_2, k_3,

Table 2 Force proportion experiments and results

Exp. no.	$h_{\max}$ (µm)	V_S (m/s)	Ductile ground surface (%)	
			Experiments	Model calculation
1	0.16	140	95.25	97.8
2	0.30	140	85	81.5
3	1.04	140	55	51.1
4	1.8	140	39	42.0
5	1.04	80	54.25	51.8
6	1.04	20	58.25	53.5
7	0.60	80	58	63.0
8	0.52	20	62	68.6
9	0.60	80	61	63.0
10	0.52	80	64.75	66.5

Table 3 Crack size experiments and results

Exp. no.	$h_{\max}$ (µm)	V_S (m/s)	Crack size (µm)	
			Experiments	Model calculation
1	0.52	20	95	85
2	0.52	140	42	47
3	1.04	20	103	99
4	1.04	80	65	68
5	0.87	80	65	58
6	1.8	140	74	68
7	0.60	80	52	57
8	0.89	20	89	94
9	0.52	80	58	55
10	1.04	140	57	58

Table 4 Experimental conditions for model calibration

Exp. no.	a_e (μm)	V_W (m/s)	V_S (m/s)	Exp. no.	a_e (μm)	V_W (m/s)	V_S (m/s)
1	5	0.1	20	11	3	0.025	20
2	5	0.1	120	12	5.2	0.075	20
3	5	0.1	100	13	5	0.1	40
4	8	0.1	100	14	5	0.1	80
5	5	0.24	100	15	5	0.16	100
6	12	0.2	120	16	8	0.15	100
7	8	0.1	20	17	12	0.3	120
8	8	0.2	40	18	8	0.4	80
9	8	0.5	100	19	8	0.6	120
10	8	0.7	140	20	3	0.1	80

and k_5 will be determined through experimental results in Fig. 4. Through calculation, the three parameters are, 4.25, 140935, and 3.5, respectively.

For validation of this grinding model, a total of 8 different experiments were performed. The process parameters, including depth of cut a_e, the wheel speed V_S, and the workpiece peripheral speed V_W, are given in the Table 4, No. 13–20. The experimental and predictive normal force and tangential force are given in Figs. 5 and 6. From the two figures, it can be found that the predictive force matches very well with the experimental results. The average percentage of error in the normal force and tangential force was 5.3 % and 6.6 %.

6 Conclusions

Grinding of brittle materials is characterized by a complex removal mechanism of both ductile and brittle removal. A model to predict the grinding force of brittle material has been developed and validated. This force model considered the co-existing of ductility and brittleness for grinding of brittle materials. The ductile removal force was modeled incorporating rubbing force, ploughing force, and chipping force, while the brittle removal force is concerned about rubbing force and fracture chipping force.

The proportional coefficient of ductile removal has been modeled and validated through a series of SEM investigations on the ground surface by a grid interface sectioning technique. Moreover, the fracture cracks model will further help to predict the chipping force in brittle grinding. The working status for a single grit has been divided based on the Hertz Theory and chip thickness modeling of Rayleigh probability density function.

Grinding experiments have been undertaken to establish and validate the model for proportional coefficient δ and crack size C. The results show that the predictive grinding force model can be successfully used in force prediction of brittle material. The predictive force model shows reasonable agreement quantitatively with the experimental force data.

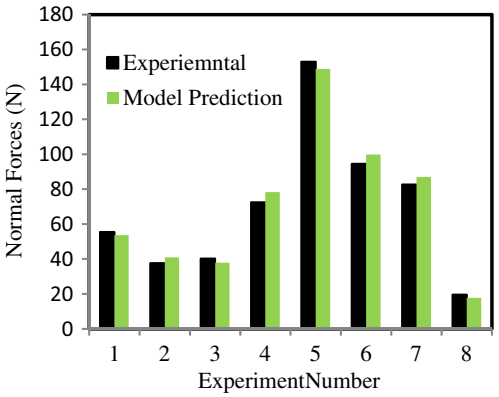

Fig. 5 Normal force for validation

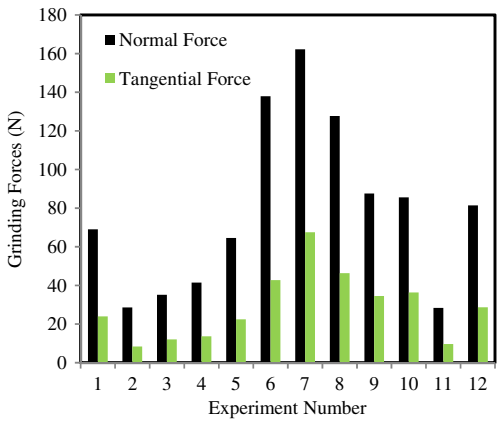

Fig. 4 Experimental results for calibration of the force model

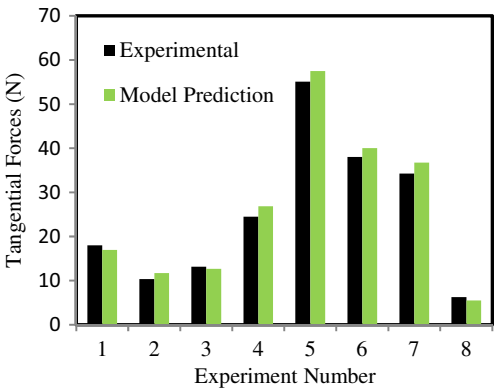

Fig. 6 Tangential force for validation

Acknowledgments This work is supported in part by the National High Technology Research and Development Program of China (2012AA041309), Innovation Funds of Donghua University (CUSF-DH-D-2015100) and Morris M. Bryan Jr. Professorship for Advanced Manufacturing Systems. The authors wish to record their gratitude for their generous support.

References

1. Feng J, Chen P, Ni J (2013) Prediction of grinding force in microgrinding of ceramic materials by cohesive zone-based finite element method. Int J Adv Manuf Technol 68:1039–1053
2. Li B, Ni J, Yang J (2014) Study on high-speed grinding mechanisms for quality and process efficiency. Int J Adv Manuf Technol 70(5–8):813–819
3. Ming Z, Wang XJ, Ngoi BKA, Gan JGK (2002) Brittle–ductile transition in the diamond cutting of glasses with the aid of ultrasonic vibration. J Mater Process Technol 121(2–3):243–251
4. Lin S, Yang S, Lin Y, Zhao P, Wu P, Jiang Z (2015) A new model of grinding forces prediction for machining brittle and hard materials. Procedia CIRP 27:192–197
5. Ramesh K, Yeo SH, Gowri S, Zhou L (2001) Experimental evaluation of super high-speed grinding of advanced ceramics. Int J Adv Manuf Technol 17:87–92
6. Yao L, Beizhi L, Chongjun W, Yihao Z (2015) Simulation-based evaluation of surface micro-cracks and fracture toughness in high-speed grinding of silicon carbide ceramics. Int J Adv Manuf Technol. doi:10.1007/s00170-015-8218–4
7. Brinksmeier E, Mutlugünes Y, Klocke F, Aurich JC, Shore P, Ohmori H (2010) Ultra-precision grinding. CIRP Ann Manuf Technol 59(2):652–671
8. Wang ZG, Cheng X, Nakamoto K, Kobayashi S, Yamazaki K (2010) Design and development of a precision machine tool using counter motion mechanisms. International Journal of Machine Tools and Manufacture. Volume 50, Issue 4
9. Hecker RL, Liang SY, Wu XJ, Xia P, Guo D, Wei J (2007) Grinding force and power modeling based on chip thickness analysis. Int J Adv Manuf Technol 33(5–6):449–459
10. Malkin S, Cook NH (1971) The wear of grinding wheels, part 1, attritious wear. Transactions of the ASME. J Eng Ind Series B 93: 1120–1133
11. Badger JA, Torrance AA (2000) A comparison of two models to predict grinding forces from wheel surface topography. Int J Mach Tools Manuf 40(8):1099–1120
12. Patnaik Durgumahanti US, Singh V, Venkateswara Rao P (2010) A new model for grinding force prediction and analysis. Int J Mach Tools Manuf 5:231–240
13. Bifano TG, Dow TA, Scattergood RO (1991) Ductile-regime grinding: a new technology for machining brittle materials. J Eng Ind Trans ASME 113(2):184–189
14. Sanjay A, Venkateswara Rao P (2013) Predictive modeling of force and power based on a new analytical undeformed chip thickness model in ceramic grinding. Int J Mach Tools Manuf 65:68–78
15. Xu HHK, Jahanmir S, Ives LK (1997) Effect of grinding on strength of tetragonal zirconia and zirconia toughened alumina. Mach Sci Technol 1(1):49–66
16. Malkin S (1989) Grinding technology, theory and applications of machining with abrasives. Ellis Horwood Limited, Chichester
17. Jiaming N, Beizhi L, Jingzhu P (2013) High-speed cylindrical grinding of SiC: the process characteristics and surface integrity. J Cer Proc Res 14(1):70–76
18. Cao J, Wu Y b, Jianyong L, Qinjian Z (2015) A grinding force model for ultrasonic assisted internal grinding (UAIG) of SiC ceramics. Int J Adv Manuf Technol 81:875–885
19. Subhash, G. and Ravichandran, G (1993) Mechanical behavior of hot pressed aluminum nitride under uniaxial compression, Graduate Aeronautical Labs, California Inst. of Technology, SM Report 93–7
20. Shih CJ, Meyers MA, Nesterenko VF, Chen SJ (2000) Damage evolution in dynamic deformation of silicon carbide. Acta Mater 48:2399–2420
21. Lal GK, Brecker JN, Sauer WJ, Shaw MC (1970) Fifth Annual Report on Abrasive Grain Association Investigation of Abrasive Grain Characteristics, Carnegie Institute of Technology
22. Greenwood JA, Johnson KL, Matsubara E (1984) A surface roughness parameter in Hertz contact. Wear 100(1–3):47–57
23. De Vathaire M, Delamare F, Felder E (1981) An upper bound model of ploughing by a pyramidal indenter. Wear 66:55–64
24. Lawn BR, Evans AG (1980) Elastic/plastic indentation damage in ceramics: the median/radial crack system. J Amer Ceram, SOC 63: 574–581
25. Hecker RL, Ramoneda I, Liang SY (2003) Static and dynamic wheel microstructure characterization. Trans North Am Manuf Res Inst Soc Manuf Eng
26. Xu HHK, Jahanmir S (1994) Simple technique for observing subsurface damage in machining of ceramics. J Am Ceram Soc 77: 1388–1390
27. Blake PN, Scattergood RO (1990) Ductile-regime machining of germanium and silicon. J Am Ceram Soc 73(4):949–957
28. Kovach JA, Malkin S (1993) A feasibility investigation of high-speed, low-damage grinding for advanced ceramics, Society of Manufacturing Engineers, Cincinnati, Ohio, MR93-352